Journal of Applied Electrochemistry **29**: 979–986, 1999.

Evaluation of the surface roughness of microporous Ni–Zn–P electrodes by *in situ* methods

R. KARIMI SHERVEDANI and A. LASIA
Département de Chimie, Université de Sherbrooke, Sherbrooke, Québec, J1K 2R1, Canada

Received 3 September 1998; accepted in revised form 14 January 1999

Key words: CO oxidation, electrode capacitance, hydrogen evolution reaction, nickel based electrodes, surface roughness

Abstract

The surface roughness of porous Ni–Zn–P electrodes was studied in 1 M NaOH using *in situ* electrochemical techniques: ratio of the polarization current densities, electrochemical impedance spectroscopy, cyclic voltammetry, coulometric oxidation of the surface, and a new technique of a CO molecular probe. The obtained surface roughness was about 5.5×10^3. Good agreement was observed between the results obtained by all these techniques.

1. Introduction

Evaluation of the roughness factor, R, of the electrode is indispensable in electrocatalysis, particularly in studies of the reaction mechanisms and kinetics and the determination of the intrinsic activities of electrode materials. *In situ* and *ex situ* methods [1, 2] may be applied. *In situ* methods are preferred because the surface properties may change upon drying the electrode material, however, there are no good techniques for the surface roughness determination. For very porous electrodes a precise value of the roughness factor is usually not necessary and a roughly estimated value is usually sufficient.

Various methods have been previously applied to determine the real surface area of the electrodes. For example, it has been determined from the double layer capacitance using cyclic voltammetry [1, 2] or EIS [3–6], from initial potential-decay curve slopes [4–6], from a comparison of the steady-state currents due to the HER at a constant overpotential [7, 8], from the charge of nickel oxidation using voltammetric [9, 10] or chronopotentiometric [8] techniques, or from the current corresponding to a redox process in solution [11]. However, different techniques (i.e., more than two) are rarely compared in one paper.

For some noble metals the charge of the hydrogen underpotential deposition (UPD) may be used for the determination of the surface area [12]. The use of the overpotentially deposited hydrogen (OPD) was also suggested in the literature [13] but this method cannot give correct results because the OPD hydrogen coverage is, in general, lower than one and it depends on the reaction rate constants [3, 14]. Moreover, during the desorption (discharge) process the Volmer and Heyrovsky reactions proceed in opposite directions but only the net current may be recorded. In some cases the Tafel reaction may also proceed during the discharge decreasing the amount of adsorbed hydrogen and causing further errors.

CO adsorbs on nickel surface and it may be oxidized to CO_2 [15–18]. It was suggested that such an oxidation is not quantitative in acidic solutions [17] and the coulometric results in alkaline solutions were not conclusive. This reaction could, in principle, be used for the determination of the total surface area.

The purpose of the present paper is the comparison of several *in situ* methods for the determination of the real surface area or surface roughness factors of nickel based electrodes. For these studies we have chosen a recently developed Raney-type Ni–Zn–P electrode [19], which is active, stable and easily prepared by electroplating; it is also characterized by a large real surface area. The surface may be easily changed by changing the leachable zinc content. Several methods were tested: electrochemical impedance spectroscopy (EIS), coulometric oxidation of the surface, cyclic voltammetry (CV), ratio of the hydrogen evolution currents, and oxidation of CO adsorbed on the electrode surface.

2. Experimental details

The Ni–Zn–P electrodes were prepared in three steps by electrodepositing subsequently layers of Ni, Ni–P and Ni–Zn–P with the content gradient of Zn, as described elsewhere [19], but the electrodeposition was carried out at a higher temperature, 75 °C, and a lower current density, 50 mA cm^{-2}. After deposition the electrodes were removed and leached in 30% KOH at 70 °C for 24 h. The composition and surface morphology of the electrodes was studied by EDX-SEM [19] using external standards.

All measurements were performed in 1 M NaOH (Aldrich, 99.99%) using Barnstead Nanopure water (17.7 MΩ cm). The instruments, cell, counter and reference electrodes were the same as in our previous work [19]. Carbon monoxide was from Linde Co., Union Carbide. All measurements were performed at 70 °C except those with CO which were carried out at 25 °C. The reference electrode was Hg/HgO/1 M NaOH at room temperature.

All the measurements were performed after obtaining reproducible polarization (Tafel) curves. These conditions were obtained approximately after 24 h of the HER at a constant current density of 320 mA cm^{-2}. The Tafel plots were recorded galvanostatically (45 s after application of a constant current) at cathodic current densities ranging from 320 mA cm^{-2} to 0.04 μA cm^{-2}. At the steady-state, the electrode potentials were corrected for iR_s drop, determined by the EIS technique at various electrode potentials. The EIS measurements and data modelling are described in our earlier papers [3, 19, 20].

In the coulometric oxidation studies the electrode was subjected to a cathodic current of 2 mA cm^{-2} for 5 min followed by application of the anodic current of 2 mA cm^{-2}, during which the electrode potential was recorded as a function of time. It was assumed that the charge necessary to oxidize a monolayer of Ni to $Ni(OH)_2$ is 0.463 mC cm^{-2} [9].

Cyclic voltammetric studies were performed in the potential range −0.810 to −1.000 V vs Hg/HgO with different scan rate at 70 °C in 1 M NaOH. The voltammetric curves were measured using a digitally generated potential sweep using EG&G M270 software and also an analog sweep generator EG&G PAR 175 and a Headstart software.

The measurements were performed on a polycrystalline Ni and porous Ni–Zn–P electrodes. Before each experiment Ni electrode was polished with 0.05 μm alumina (Buehler®, Gamma Micropolish®), washed with water, 1:5 H_2SO_4 solution, again with water (deoxygenated with nitrogen), connected to the cathodic potential immediately and then introduced to the cell. The electrode was kept near the hydrogen evolution equilibrium potential of −0.935 V vs Hg/HgO for half an hour under N_2 atmosphere.

The electrode was cycled between −0.930 and 0.200 V (starting at −0.93 V) and the first and second cyclic voltammograms were recorded. For measurements of CO adsorption the freshly prepared Ni electrode was washed with 1 M NaOH, deoxygenated with N_2 and saturated with CO, and introduced to the cell under the HER equilibrium potential. The solution was bubbled with CO for 25 min and CO was passed over the solution during the measurements. The measurements were carried out also after bubbling with CO for 25 min and then with N_2 for 25 or 100 min.

In other experiments the CO saturated solution was drained out and replaced by a pure and deoxygenated 1 M NaOH, bubbled one hour with N_2, and then N_2 was passed over the solution. Identical results were obtained in these conditions.

The experiments in the presence of CO were performed similarly to those with polycrystalline Ni but, initially, the electrode was polarized for 24 h at a constant cathodic current of 320 mA cm^{-2} and the time of bubbling with N_2 and CO was increased to 2.5 h. A freshly prepared electrode was used for each CV experiment.

3. Results

3.1. *Electrode composition and surface morphology*

The electrode composed of three layers of Ni, Ni–P and Ni–Zn–P, their thickness was 70, 30 and 20 μm, respectively. The surface composition of the electrode was $Ni_{66}Zn_{14}P_{20}$ before and $Ni_{86}Zn_2P_{12}$ after leaching, obtained by EDX quantitative analysis. Because the electrolysis still continued 15 min after addition of the total amount of zinc this composition characterizes the topmost layer. Of course the strict surface composition may be different and it should be studied by surface sensitive methods. The appearance of the electrode was similar to that presented earlier for $Ni_{54}Zn_{20}P_{26}$ electrode [19]. In the text below the electrode is indicated as $Ni_{66}Zn_{14}P_{20}$, but all the electrochemical measurements were performed on leached electrodes.

3.2. *Evaluation of the surface roughness by* in situ *methods*

3.2.1. *Ratio of the polarization current densities*

Figure 1 presents the steady-state polarization curves obtained on $Ni_{66}Zn_{14}P_{20}$ electrode at different polarization times per point at 70 °C in 1 M NaOH saturated

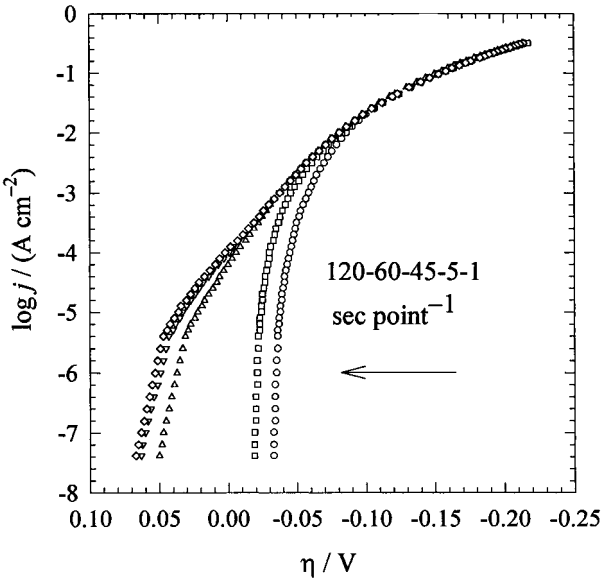

Fig. 1. Steady-state polarization curves obtained for the HER on $Ni_{66}Zn_{14}P_{20}$ electrode in 1 M NaOH at 70 °C in N_2 atmosphere at times after application of a constant current.

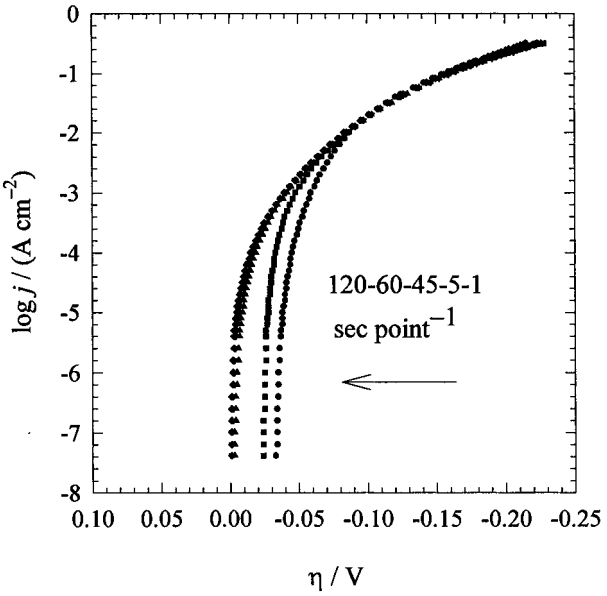

Fig. 2. Steady-state polarization curves obtained in the similar conditions as in Figure 1 but in the H_2 atmosphere.

with N_2. These electrodes were characterized by the exchange current density $j_0 = 2.5 \times 10^{-4}$ A cm^{-2}, the slope $b = -72$ mV dec^{-1}, and the overpotential at 250 mA cm^{-2}, $\eta_{250} = -163$ mV (at 45 s per point). At more positive potentials another slope of -33 mV dec^{-1} was observed. Since a part of the curve extended to positive overpotentials, it could not be related to the HER. As waiting time at each current density increased from 1 to 120 s the open-circuit potential shifted from negative to positive overpotentials. This behaviour is connected with the absence of hydrogen in the solution ($p_{H_2} \to 0$). In such conditions H_2/H_2O equilibrium potential cannot be reached and a mixed/corrosion potential is observed. Figure 2 presents the Tafel plots in the solution saturated with H_2. In this case the equilibrium potential is shifted towards more negative values and becomes equal, at longer times, to that of the HER. The obtained results indicate that low Tafel slopes observed at low currents are artifacts caused by a lack of hydrogen in solution around the electrode. Only in the presence of hydrogen, at sufficiently long times, the correct Tafel curves may be obtained.

Comparison of the HER currents at the same overvoltage at a porous/rough and smooth nickel electrode was suggested in the literature to determine the surface area [7, 8]. Comparison of currents at $\eta = -173$ mV at $Ni_{66}Zn_{14}P_{20}$ and a smooth Ni electrodes gives $j_{1\eta} = 318$ and $j_{2\eta} = 0.16$ mA cm^{-2}, respectively. Assuming that the surface roughness of polycrystalline Ni is ~2 [21], this leads to the surface roughness $R = j_{1\eta}/(j_{2\eta}/2) \sim 4 \times 10^3$. At $\eta = -128$ mV the roughness factor is 2.2×10^3. However, this method may be used only when the transfer coefficients and intrinsic activities of two electrodes studied are the same. In the present case the transfer coefficients (or Tafel slopes) are different and this method cannot give precise results. Despite these limitations it was used in the literature [7, 8].

3.2.2. *Electrochemical impedance spectroscopy*

The surface roughness may be obtained by comparing the double layer capacitance of porous/rough and smooth electrode. The behaviour of $Ni_{66}Zn_{14}P_{20}$ electrodes in the EIS was similar to those reported in our previous paper [19], the complex plane plots corresponded to the porous electrode behaviour [3, 14, 19, 22] that is a line at 45° at high frequencies (a very small part observed on the complex plane plots) followed by a semicircle at low frequencies. Approximation of data was achieved using a modified porous model [22] in which the double layer capacitance was substituted by a constant phase element. The average double layer capacitances $\bar{C}_{dl}$, were obtained using formula suggested by Brug et al. [23] and successfully used in further papers [3, 14, 19, 21, 22] Figures 3 and 4 presents examples of the complex plane and Bode plots obtained on Ni–Zn–P electrodes. The average double layer capacitance obtained at the HER potentials is ~0.128 mF cm^{-2}, which leads to a roughness factor $R = 6.4 \times 10^3$, assuming the double layer capacitance of

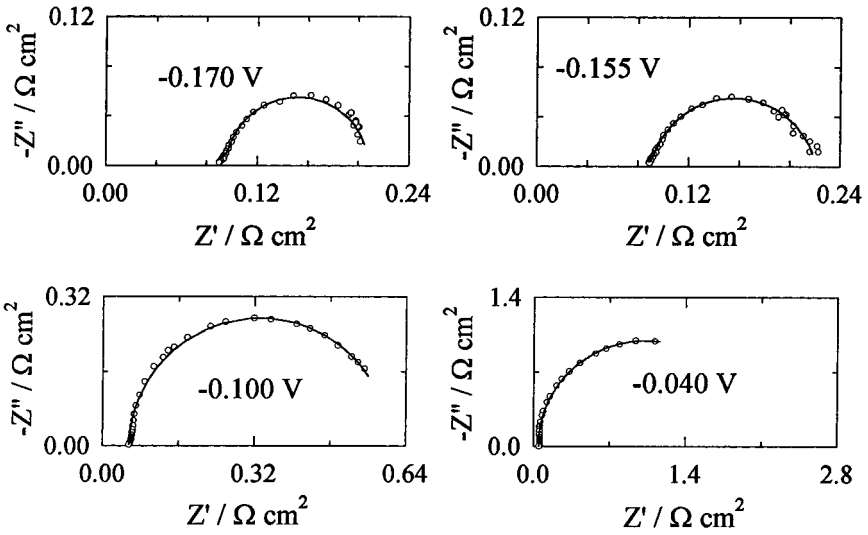

Fig. 3. Complex plane plots obtained on $Ni_{66}Zn_{14}P_{20}$ in 1 M NaOH at 70 °C. Continuous lines are obtained from the fit using the CNLS method.

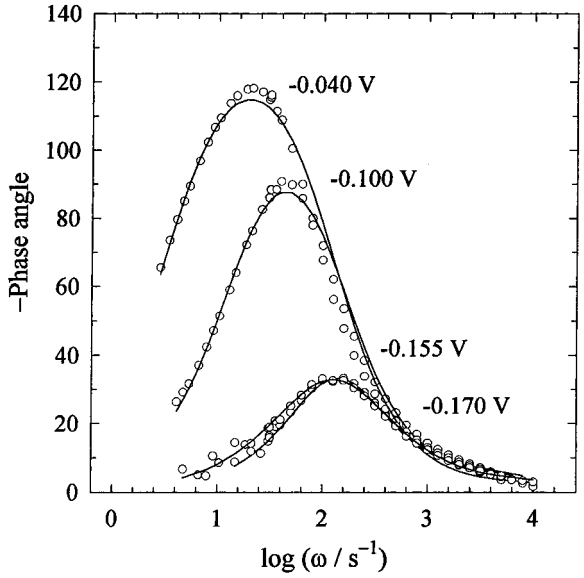

Fig. 4. Phase angle Bode plots for $Ni_{66}Zn_{14}P_{20}$. Details as specified for Figure 3.

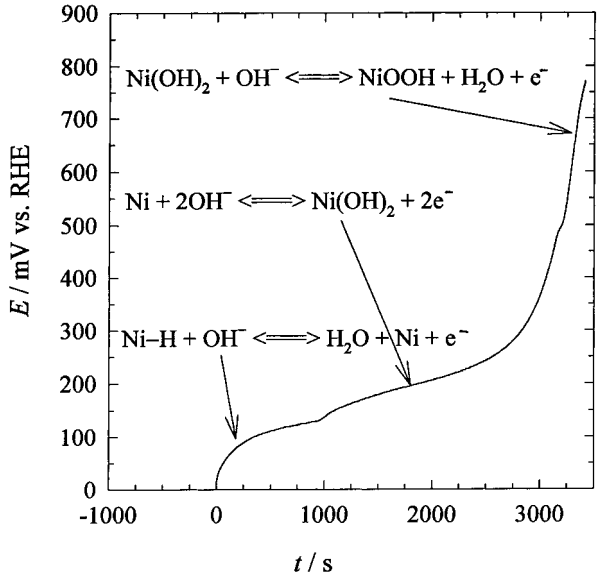

Fig. 5. Charging curve of $Ni_{66}Zn_{14}P_{20}$ electrode in 1 M NaOH at 70 °C, $j = -2\,mA\,cm^{-2}$ (anodic current).

a smooth Ni surface as equal to 20 $\mu F\ cm^{-2}$ [3, 14, 19, 21, 22].

3.2.3. *Coulometric method*

The $Ni_{66}Zn_{14}P_{20}$ charging curve consists of three parts [8], Figure 5. The first part corresponds to the oxidation of adsorbed hydrogen (from 0.0 to about 120 mV vs RHE), the second part is attributed to the oxidation reaction of Ni to $Ni(OH)_2$ (from about 120 to about 300 mV vs RHE). This part was followed by a large increase in the electrode potential which implies the transition of $Ni(OH)_2$ to NiOOH. It has been suggested [8] that the total charge consumed in the second range is related to the formation of one monolayer of $Ni(OH)_2$ on the Raney nickel electrodes [8–10]. The charge obtained for nickel oxidation is 3.98 C cm^{-2} which corresponds to the roughness factor of 8.6×10^3 assuming that the charge corresponding the formation of a monolayer of $Ni(OH)_2$ 4.63×10^{-4} C cm^{-2} [9].

3.2.4. *Cyclic voltammetry*

Cyclic voltammograms were obtained using analogue potential sweep generation and different digital acquisition modes (AM) available in EG&G M270 program: 1/4, 2/4, 3/4 and 4/4, at different sweep rates. Examples of the CV curves obtained using different methods are displayed in Figure 6. A plateau region was observed between −0.820 to −0.950 V vs Hg/HgO. The capacitive current densities were extracted using average current density, $j_{dl} = (j_a + j_c)/2$, at −0.910 V vs Hg/HgO, where j_a and j_c are the anodic and cathodic capacitive current densities. The dependence of j_{dl} on the sweep rate is presented in Figure 7. The double layer capacitances obtained varied from 0.07 to 0.04 F cm^{-2}. It is obvious that the different acquisition modes lead to different capacitances and the largest value was obtained using the analogue signal. This phenomenon is connected with the fact that digitally generated sweep consists of the potential steps after which the capacitive current decreases exponentially. These results indicate that popular programs which use digitally generated sweeps should not be applied to determine the capacitive electrode behaviour. The roughness factor obtained using the analogue sweep is 3.5×10^3.

3.2.5. *Adsorption of carbon monoxide*

(a) *Ni electrodes*. Figure 8, curve 1, presents the first cyclic voltammogram obtained on Ni in the absence of CO. A flat irreversible peak around −0.490 V is attributed to the oxidation of nickel [15–17]. Figure 8, curve 2 presents the first cyclic voltammogram of Ni oxidation in the solution saturated with CO. Large peak is observed, it decreases after bubbling the solution with N_2 for 25 min, curve 3. When the bubbling continues for 100 min the peak decreased further, curve 4. Bubbling for longer time does not change the peak area. These results indicate that dissolved CO is oxidized at the same potential as adsorbed CO. The experiment was also carried out after adsorbing CO on the electrode surface and then replacing the solution containing CO with a new CO free solution and bubbling with N_2 for 1 h. The obtained curve was identical to that shown in Figure 8, curve 4. The second sweeps were the same in all the cases, Figure 8, curve 5. This result implies that β-Ni(OH)$_2$ is formed on the electrode surface in such conditions, which cannot be reduced. The charge under anodic peak around −0.380 mV (Fig. 8, curve 4) may be attributed to the oxidation of adsorbed CO and nickel. Curve 2 corresponds to the oxidation of nickel and CO adsorbed and dissolved in the solution.

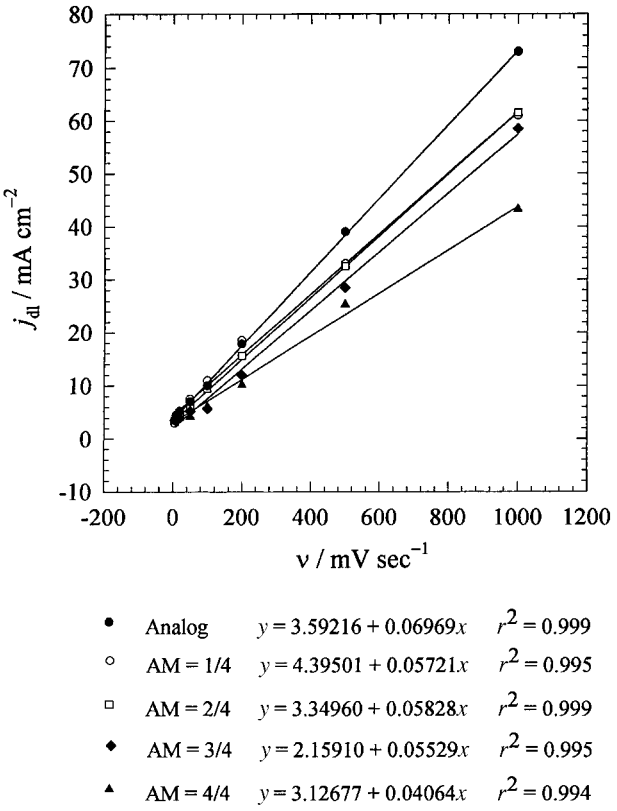

Fig. 7. Dependence of the capacitive current density on $Ni_{66}Zn_{14}P_{20}$ electrode at −0.910 V on sweep rate at 70 °C in 1 M NaOH: analogue (●), and digital acquisition modes, AM, in EG&G M270 software; (○) 1/4, (□) 2/4, (▲) 3/4 and (◆) 4/4. Slope indicates the double layer capacitance and r^2 is the determination coefficient.

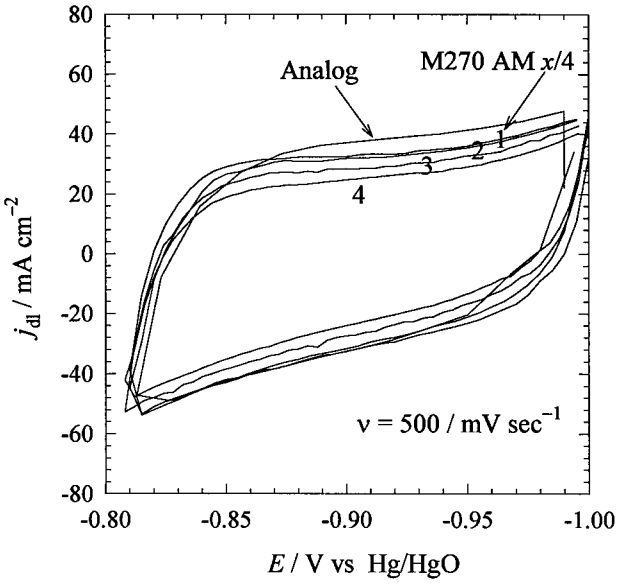

Fig. 6. Cyclic voltammograms obtained on $Ni_{66}Zn_{14}P_{20}$ electrodes at 70 °C in 1 M NaOH at 500 mV s^{-1} using different data acquisition modes (AM x/4, x from 1 to 4) in M270 software and analog potential sweep generation.

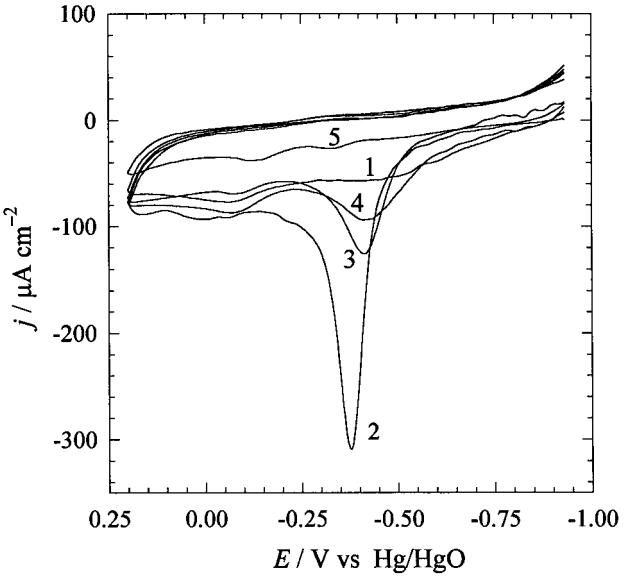

Fig. 8. Cyclic voltammograms obtained on polycrystalline nickel electrode at 25 °C in 1 M NaOH, scan rate 20 mV s^{-1}; (1) the first cycle in the absence of CO, (2) in the solution saturated with CO, (3) after 25 min bubbling with CO followed by 25 min bubbling with N_2, (4) after 25 min bubbling with CO followed by 100 min bubbling with N_2 or replacing the solution by a new and deoxygenated pure 1 M NaOH and (5) the second cycles for all the cases.

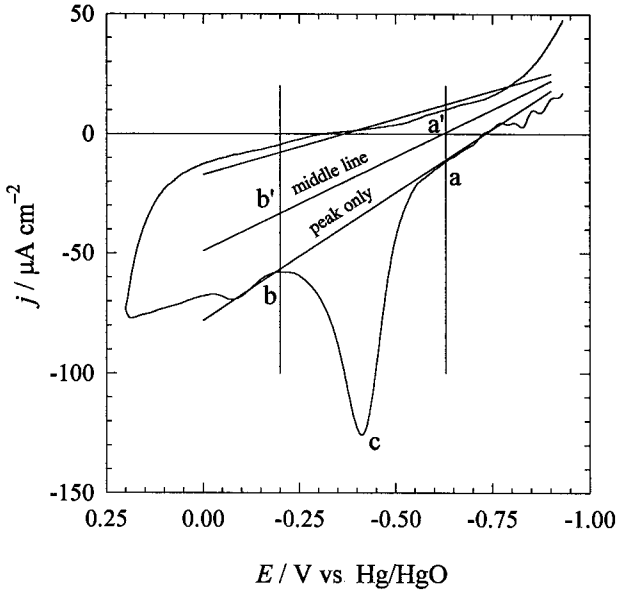

Fig. 9. A typical cyclic voltammogram selected from Figure 8 (curve 3) showing two base lines for data integration: only peak (from a–b line) and the total area (form a′–b′ line).

Considering that the total charge for oxidation of one monolayer of Ni electrode is 0.463 mC cm^{-2} and one CO molecule is adsorbed on each surface Ni atom the charge for oxidation of one monolayer of CO and Ni is 0.926 mC cm^{-2}. The total charge may be obtained by integration of the voltammetric current. However, there is a problem in the determination of the baseline for integration, Figure 9. The current observed outside the peak is much larger than the capacitive current at this sweep rate and the peak charge measured from the line a–b is much smaller than theoretically predicted for the oxidation of a monolayer, Table 2. Therefore, the charge was determined from the line a′–b′, traced in the middle between the anodic and cathodic base lines. The calculated capacitive charge for polycrystalline Ni is of the order of 0.017 mC cm^{-2} while the total charge determined from curve 4 in Figure 8 (between lines b–b′ and a–a′) was 1.17 mC cm^{-2}. It gave the roughness factor R of 1.26. The oxidation reaction maybe written as

$$Ni(CO)_{ad} + 6\,OH^- \rightarrow Ni(OH)_{2,ad} + CO_3^{2-} + 2\,H_2O + 4\,e^-$$

Table 1. Double layer capacitances, C_{dl}, and roughness factors, R, obtained on $Ni_{66}Zn_{14}P_{20}$ in 1 M NaOH using different techniques

Method	C_{dl}/F cm^{-2}	R
EIS	0.128	6.4×10^3
Coulometric Ni(II)/Ni		8.6×10^3
Tafel plot		5.0×10^3
CV (analogue)	0.070	3.5×10^3
CO		4.2×10^3
Average		$(5.5 \pm 2.0) \times 10^3$

Table 2. Charges of CO and Ni electrooxidation and surface roughness obtained on polycrystalline Ni electrode in 1 M NaOH at 25 °C Two methods of integration are displayed in Figure 9

Conditions	Q_1/mC cm^{-2} from a′–b′	Q_2/mC cm^{-2} from a–b	Q_1/Q_{01}	Q_2/Q_{02}	R
Deoxygenated solution	$Q_{01} = 0.65$	$Q_{02} = 0.203$	1.0	1.0	1.41
CO saturated	2.15	1.32	3.3	6.5	2.33
CO + 25 min of N_2	1.2	0.67	1.85	3.3	1.3
CO + replacing with deoxygenated solution	1.17	0.54	1.8	2.7	1.3

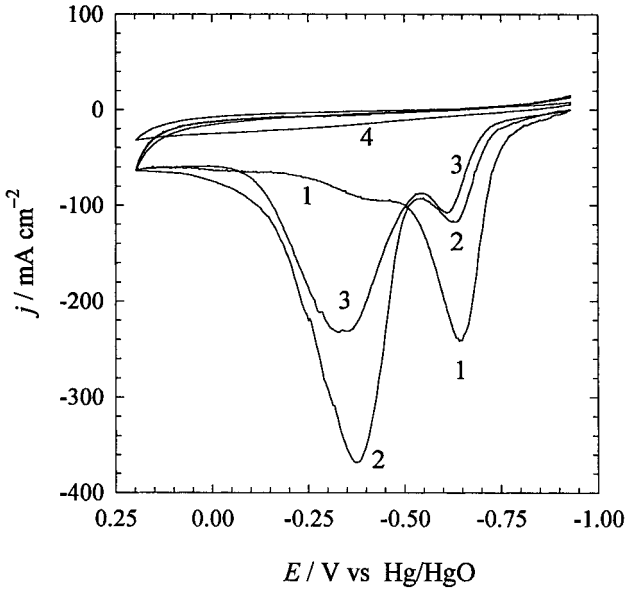

Fig. 10. Cyclic voltammograms obtained on $Ni_{66}Zn_{14}P_{20}$ at 25 °C in 1 M NaOH and 20 mV s^{-1} scan rate; the first cycles: (1) in the absence of CO, (2) after 2.5 h bubbling with CO, and (3) after 2.5 h bubbling with CO followed by replacing the solution with a new and deoxygenated pure solution of 1 M NaOH. (4) Second cycles for all cases.

(b) *Adsorption of CO on Ni–Zn–P electrodes*. Subsequently, the same technique was applied to the porous nickel electrode. Figure 10 displays the cyclic voltammograms obtained on $Ni_{66}Zn_{14}P_{20}$ electrodes in 1 M NaOH at 25 °C at different conditions. The charge under anodic Ni oxidation peak in the absence of CO was 2.03 C cm^{-2}, Figure 10, curve 1 and Table 3. When the solution was saturated with CO two peaks were obtained, one at the same potential as that of Ni oxidation, the second at more positive potentials, curve 2. The total charge under these peaks is 5.70 C cm^{-2}. After replacing the solution containing CO with a new one saturated wit N_2, the peak at −0.35 V decreased, curve 3, and the total anodic charge under two peaks was 3.88 C cm^{-2}. The ratio of the anodic peaks of curves 1 and 3 was 1.9, which is close to the value of 2 predicted for the stoichiometry Ni:CO equal 1:1. This result leads to the surface roughness factor of 4.2×10^3. The presence of two anodic peaks in the presence of CO may be attributed to the fact that some part of nickel surface is not covered by CO (e.g., in deep pores) or to the presence of different centres characterized by different CO adsorption energy. Assuming that the more negative peak is connected with the nickel oxidation only, its charge is 0.57 C cm^{-2} and adjusting for the different oxidation stoichiometry leads to a slightly larger surface roughness factor of 4.35×10^3.

4. Discussion

The surface roughness of Ni and alkali-leached Ni–Zn–P electrodes was determined *in situ* by several electrochemical techniques at the positive potentials (coulometric oxidation, CV, adsorption of CO) and negative (HER current comparison, EIS) of the HER equilibrium potential. It should be stressed that some methods (Ni and Ni + CO oxidation) are specific for nickel based electrodes. The results are shown in Table 1. The average value of the surface roughness is $(5.5 \pm 2.0) \times 10^3$. Between the techniques used the most doubtful is the comparison of the HER currents at the same overvoltage. It assumes the same Tafel slopes and intrinsic activities of the Raney and polycrystalline nickel electrodes. However, the Tafel slope obtained on Ni–Zn–P electrodes is −72 mV dec^{-1} and that on polycrystalline Ni −115 mV dec^{-1} [21]. Nevertheless, the results obtained by this method are similar to those obtained by other techniques.

The results obtained indicate that the steady-state polarization experiments should be carried out after obtaining stationary conditions in the solution saturated with hydrogen. When the solution is bubbled by nitrogen a new linear part on the Tafel plots is obtained (connected with corrosion/mixed potential). Such an artefact may also be observed when a slow potential sweep is used to obtain the Tafel plots.

The CV technique is limited to a narrow potential range between the HER and nickel oxidation. It should

Table 3. Charges of CO and Ni electrooxidation and surface roughness obtained on $Ni_{66}Zn_{14}P_{20}$ electrode in 1 M NaOH at 25 °C

Conditions	Q_1/C cm^{-2} from a′–b′	Q_2/C cm^{-2} from a–b	Q_1/Q_{01}	Q_2/Q_{02}	R	R/R_{EIS}
Deoxygenated solution	$Q_{01} = 2.03$	$Q_{02} = 1.56$	1.0	1.0	4.4×10^3	0.69
CO saturated	5.70	4.69	2.8	3	6.2×10^3	0.96
CO + replacing with deoxygenated solution	3.88	3.09	1.9	2	4.2×10^3	0.66

be stressed that an analogue potential sweep generator should be used in such experiments as the digitally generated step sweep leads to lower capacitances.

The coulometric oxidation technique agrees with the others. However, Rausch and Wendt [8] obtained surface roughness of Ni–Zn electrodes about 10 times larger using this technique in comparison with the EIS. It is not clear what caused this difference.

The new CO molecular probe technique also works well. The comparison of charges indicate that nickel and adsorbed CO are both oxidized during the anodic potential sweep. On porous nickel the oxidation of CO takes place at the potentials more positive than oxidation of Ni. On polycrystalline Ni the nickel oxidation peak is more flat, however, the charges agree well with the surface roughness. This technique is better suited to determine the roughness factor of porous electrodes.

EIS is the probably the most popular non destructive technique for the surface roughness determination. It also gives relatively good results. The techniques based on the electrode oxidation involve irreversible oxidation of Ni to $Ni(OH)_2$ and destruction of the electrode. The use of a few different techniques is recommended for the real surface area or surface roughness factor determinations.

Acknowledgements

Financial support from the Chair on Hydrogen (Ministère des Ressources Naturelles du Québec) and the Ministry of Culture and Higher Education of Iran, MCHE (grant for R. Karimi Shervedani) is gratefully acknowledged.

References

1. S. Trasatti and O.A. Petrii, *Pure Appl. Chem.* **63** (1991) 711.
2. A.T. Kuhn, In: A.T. Kuhn (ed.) *Techniques in Electrochemistry, Corrosion and Metal Finishing*, J. Wiley & Sons, Chichester, (1987) p. 95.
3. A. Lasia, *Current Topics Electrochem.* **2** (1993) 239.
4. P. Gu, L. Bai, R. Brousseau and B.E. Conway, *Electochim. Acta.* **37** (1992) 2145.
5. L. Bai, L. Gao and B.E. Conway, *J. Chem. Soc. Faraday Trans.* **89** (1993) 235.
6. R. Šimpraga, G. Tremiliosi-Filho, S.Y. Qian and B.E. Conway, *J. Electroanal. Chem.* **424** (1997) 141.
7. N.A. Assunção, M.J. de Giz, G. Tremiliosi-Filho and E.R. Gonzalez, *J. Electrochem. Soc.* **144** (1997) 2794.
8. S. Rauch and H. Wendt, *J. Electrochem. Soc.* **143** (1996) 2852.
9. S.A.S. Machado, J. Tiengo, P. de Lima Neto and L.A. Avaca, *Electrochim. Acta* **39** (1994) 1757.
10. S.A.S. Machado, J. Tiengo, P. de Lima Neto and L.A. Avaca, *J. Appl. Electrochem.* **26** (1996) 431.
11. C.A. Marozzi and A.C. Chialvo, *Electrochim. Acta* **41** (1996) 2351 and 2361.
12. T. Biegler, D.A.J. Rand and R. Woods, *J. Electroanal. Chem.* **29** (1971) 269.
13. J.C.K. Ho and D.L. Piron, *J. Electrochem. Soc.* **142** (1995) 1144.
14. A. Lasia, *Polish J. Chem.* **69** (1995) 639.
15. K. Wang, G.S. Chottiner and D.A. Scherson, *J. Phys. Chem.* **96** (1992) 6742.
16. M. Zhao, K. Wang and D.A. Scherson, *J. Phys. Chem.* **97** (1993) 4488.
17. C.F. Zinola, E.J. Vasini, U. Müller, H. Baltruschat and A.J. Arvia, *J. Electroanal. Chem.* **415** (1996) 165.
18. A. Cuesta and C. Gutiérrez, *J. Phys. Chem.* **100** (1996) 12600.
19. R. Karimi Shervedani and A. Lasia, *J. Electrochem. Soc.* **144** (1997) 2652.
20. R. Karimi Shervedani and A. Lasia, *J. Electrochem. Soc.* **144** (1997) 511.
21. A. Lasia and A. Rami, *J. Electroanal. Chem.* **294** (1990) 123.
22. P. Los, A. Lasia, H. Ménard and L. Brossard, *J. Electroanal. Chem.* **360** (1993) 101.
23. G.J. Brug, A.L.G. van den Eeden, M. Sluyters-Rehbach and J.H. Sluyters, *J. Electroanal. Chem.* **176** (1984) 275.